Inorganic Chemistry
Article

*Inorg. Chem.* **2009**, *48*, 5117–5128 **5117**
DOI: 10.1021/ic900394z

# Size Effects in the Oriented-Attachment Growth Process: The Case of Cu Nanoseeds

**Shuling Shen, Jing Zhuang, Xiangxing Xu, Amjad Nisar, Shi Hu, and Xun Wang***

*Department of Chemistry, Tsinghua University, Beijing, 100084, P. R. China*

Received December 18, 2008

Size effects in the oriented-attachment (OA) growth process of Cu nanoseeds were found. Monodispersed Cu nanoseeds with average diameters of 2.2, 3.4, and 5.2 nm were controllably synthesized by the reduction of copper acetate in a boiling solvent and using dodecanethiol (DT) as a stabilizer and sulfur source of sulfide. These Cu nanoseeds were then treated under solvothermal conditions. When the diameters of Cu nanoseeds were smaller than 5 nm, $Cu_2S$ nanorods with lengths of ~30−100 nm and diameters of ~2−4 nm were obtained at lower temperatures, and $Cu_2S$ nanodisks with diameters of ~6−13 nm and thicknesses of ~2−4 nm were obtained at higher temperatures. Once the diameter of Cu nanoseeds was larger than 5 nm, only irregular particles were obtained, regardless of other conditions. The uniformity, which related to the density of DT on the surface of Cu nanoseeds, was the key for success of self-assembly of the final nanocrystals. High-resolution transmission electron microscopy images demonstrated that these nanorods, nanodisks, and particles were formed by an OA process of Cu nanoseeds into 1D, 2D, and 3D aggregates, which recrystallized into single crystals.

## Introduction

Well-defined nanocrystals have attracted considerable attention in recent years due to their unique size- and shape-dependent properties and potential applications in assembling advanced materials and devices.[1] One of the main interesting and notable advances in this field is the assembly of nanocrystal building blocks into single-crystal 1D nanowires, 2D nanosheets, and other complex architectures directly via an oriented-attachment (OA) growth process.[2] While being effective in generating novel nanostructures, this OA process may also provide a deeper understanding of the growth process of nano- and microcrystals and even macrocrystals, in that it is based on the separation of nucleation and the subsequent growth process to some extent, which are usually quite difficult to discern in the normal crystal growth process. In this paper, we have synthesized Cu nanoseeds with diameters of 2, 3, and 5 nm first; then, with these nanoseeds as building blocks, OA processes were carried out under solvothermal conditions. These OA processes have proved to be size- and surface-dependent, which clearly indicates that the size and surface properties of the nanoseeds will determine the subsequent crystal growth process. This finding may serve as a new and general principle for the further investigation of crystal growth processes.

Classically, Ostwald ripening has been used extensively to describe and explain the growth of large crystals at the expense of smaller ones, driven by surface energy reduction.[3] Usually, the products grown by Ostwald ripening are nearly spherical morphologies and thermodynamically stable because of the minimization of the overall surface energy. However, the growth of particles strongly depends on the structure of the material, the properties of the solution, capping ligands, the temperature, and the interface between the particles and the surrounding environment. Recent works have shown that Ostwald ripening does not adequately describe the crystal growth for many systems, especially for the anisotropic growth of 1D nanorods or nanowires and 2D nanodisks or nanoplates.[4]

*To whom correspondence should be addressed. E-mail: wangxun@mail.tsinghua.edu.cn.

(1) (a) Bruchez, M.; Moronne, M.; Gin, P.; Weiss, S.; Alivisatos, A. P. *Science*. **1998**, *281*, 2013–2016. (b) El-Sayed, M. A. *Acc. Chem. Res*. **2004**, *37*, 326–333. (c) Li, J. J.; Wang, Y. A.; Guo, W. Z.; Keay, J. C.; Mishima, T. D.; Johnson, M. B.; Peng, X. G. *J. Am. Chem. Soc*. **2003**, *125*, 12567–12575. (d) Hyeon, T.; Lee, S. S.; Park, J.; Chung, Y.; Na, H. B. *J. Am. Chem. Soc*. **2001**, *123*, 12798–12801. (e) Collier, C. P.; Vossmeyer, T.; Heath, J. R. *Annu. Rev. Phys. Chem*. **1998**, *49*, 371–404. (f) Guo, Q.; Kim, S. J.; Kar, M.; Shafarman, W. N.; Birkmire, R. W.; Stach, E. A.; Agrawal, R.; Hillhouse, H. W. *Nano Lett*. **2008**, *8*, 2982–2987. (g) Alivistos, A. P.; Gu, W.; Larabell, C. *Annu. Rev. Biomed. Eng*. **2005**, *7*, 55–76. (h) Murray, C. B.; Sun, S.; Doyle, H.; Betley, T. *Mater. Res. Soc. Bull*. **2001**, *26*, 985–991. (i) Wang, X.; Zhuang, J; Peng, Q.; Li, Y. D. *Nature* **2005**, *437*, 121–124. (j) Shevchenko, E. V.; Ringler, M.; Schwemer, A.; Talapin, D. V.; Klar, T. A.; Rogach, A. L.; Feldmann, J.; Alivisatos, A. P. *J. Am. Chem. Soc*. **2008**, *130*, 3274–3275.

(2) (a) Yong, K. T.; Sahoo, Y.; Zeng, H.; Swihart, M. T.; Minter, J. R.; Prasad, P. N. *Chem. Mater*. **2007**, *19*, 4108–4110. (b) Tang, H.; Chang, J. C.; Shan, Y.; Lee, S. T. *J. Phys. Chem. B* **2008**, *112*, 4016–4021. (c) Liu, B.; Zeng, H. C. *J. Am. Chem. Soc*. **2004**, *126*, 8124–8125.

(3) Lifshitz, I. M.; Slyozov, V. V. *J. Phys. Chem. Solids* **1961**, *19*, 35–50.

(4) (a) Pradhan, N.; Efrima, S. *J. Phys. Chem. B* **2004**, *108*, 11964–11970. (b) Nguyen, T. D.; Mrabet, D.; Do, T. O. *J. Phys. Chem. C* **2008**, *112*, 15226–15235. (c) Lilly, G. D.; Lee, J.; Sun, Kai.; Tang, Z. Y.; Kim, K. S.; Kotov, N. A. *J. Phys. Chem. C* **2008**, *112*, 370–377.


Published on Web 05/04/2009

As a helpful complement, the view "oriented attachment", demonstrated by Penn and Banfield[5] for the first time, has been highlighted in many recent works. The growth of gold nanowires,[6] ZnO nanorods,[7] ZnS nanorods,[8] PbSe nanowires and nanorings,[9] CdTe 1D nanowires,[10] and 2D nanosheets[11] are all well-explained by the OA mechanism, which provides an efficient method for the preparation of nanocrystals with unique morphologies and controllable sizes. For the controlled OA process of nanocrystals into 1D or higher-dimensional nanostructures, surface capping ligands usually play a critical role. Polleux et al.[12] demonstrated a ligand-directed assembly of nanoparticles into anisotropic $TiO_2$ nanocrystals. Tang et al.[10] reported a similar process for CdTe nanowires. They demonstrated that the removal of excess stabilizer is the key step in the preparation of nanowires from nanoparticles. But current results show that the orientation is maintained for all nanowires produced, regardless of the initial particle size. In this article, we report the solvothermal-based synthesis of crystalline $Cu_2S$ nanorods and nonodisks using the OA growth process of Cu nanoseeds. Size effects of the Cu nanoseeds in morphology evolution during the OA process were investigated for the first time. At the same time, the OA growth characteristics determined by the surface ligand were also discussed and compared.

## Experimental Section

**Materials.** Dioctadecyldimethylammonium bromide (DODA, 99%) was purchased from Acros. The rest of the chemicals were purchased from a Beijing chemical reagent company. All chemicals were of analytical grade and were used as received without further purification. Deionized water was used throughout.

**The 2 and 3 nm Cu nanoseeds.** In a typical synthesis, 30 mg of cupric acetate and 120 mg of DODA were added into 10 mL of toluene, and the mixture was heated up to boiling under continuous magnetic stirring to form a dark green solution. An aqueous $NaBH_4$ solution (36 $\mu$L, 9.4M) was added under vigorous stirring. The dark green solution turned dark brown within a minute. A total of 36 $\mu$L of dodecanethiol (DT) was added, and the mixture was stirred at room temperature for 30 min (for ~2 nm Cu nanoseeds) and 2 h (for ~3 nm Cu nanoseeds). In order to prevent the oxidation of copper, all of the synthetic steps were carried out in a nitrogen atmosphere. Ethanol (30 mL) was added to precipitate Cu nanoseeds coated by DT (Cu-DT) with centrifugation at 10 000 rpm for 5 min. The precipitate was redispersed in toluene for the subsequent synthesis.

**The 5 nm Cu nanoseeds**[15]**.** A total of 30 mg of cupric acetate and 0.2 mL of oleic acid (OLA) were dissolved in 5 mL of toluene by heating to boiling under a nitrogen atmosphere. A total of 5 mL of $N_2H_4$ and 1 mL of OLA dissolved in 5 mL of toluene were injected, and boiling was continued for 2 h. Before the colloid solution cooled to room temperature, 36 $\mu$L of DT was injected to get ~5 nm Cu-DT nanoseeds. After the system was cooled to room temperature, 30 mL of ethanol was added to precipitate Cu-DT nanoseeds with centrifugation at 10 000 rpm for 5 min. The precipitate was redispersed in toluene for the subsequent synthesis.

**Nanorods and Rodlike Superlattice of Nanodisks.** A total of 1 mL of OLA was added to 5 mL of toluene containing 9.6 mg of Cu nanoseeds with stirring. Then, the whole mixture was transferred into a Teflon-lined autoclave of 10 mL capacity and heated at 140~200 °C. The precipitate was washed with ethanol and separated by centrifugation several times to remove residual impurities.

**Characterization.** The size, morphology, and superstructure of the nanocrystals were probed by transmission electron microscopy (TEM; JEOL JEM 1200EX working at 100 kV), high-resolution transmission electron microscopy (HRTEM; Tecnai G2 F20 S-Twin working at 200 kV), and scanning electron microscopy (SEM; JEOL JSM-6300F working at 15 kV), using a microscope equipped with an X-ray energy dispersive spectrometer (EDS). TEM samples were prepared as follows: A small amount of desired product was dispersed in toluene. One drop of the resulting suspension was deposited on carbon-coated Cu grids, and the solvent was then evaporated at room temperature in the air. UV−vis absorption spectra were measured on a Hitachi U-3010 spectrophotometer with a 1-cm quartz cuvette. Solutions were prepared typically at a concentration of 0.1 mg/mL in toluene. FT-IR spectroscopy was performed using a Nicolet 360 spectrograph with the pressed KBr pellet technique. X-ray photoelectron spectra (XPS) were recorded on a PHI Quantera SXM spectrometer using monochromatic Al Kα X-ray sources (1486.6 eV) at 2.0 kV and 20 mA. All XPS data were acquired at a nominal photoelectron takeoff angle of 45°. The binding energies of the peaks obtained were made with reference to the binding energy of the C1s line, set at 284.8 eV. The spectrum was fitted using an 80% linear combination of Gaussian−Lorentzian profiles. Powder X-ray diffraction (XRD) measurement of the products was carried out on a Bruker D8 Advance X-ray powder diffractometer with Cu Kα radiation ($\lambda$ = 1.5418 Å). $^1$H NMR spectra were recorded using a JEOL ECA-600 spectrometer. Solutions were prepared in toluene-$d_8$, and measurements were conducted at 25 °C.

## Results and Ddiscussion

**Synthesis of Cu-DT Nanoseeds with Diameters of 2, 3, and 5 nm.** The size and size distribution of highly crystalline Cu nanoseeds is the key for the subsequent investigation of the OA process. In previous reports, many methods have been developed for the synthesis of monidisperse Cu nanoparticles including microemulsion techniques,[13] the polyol method,[14] metal salt reduction,[15] electrochemical reduction,[16] and the solvothermal method.[17] However, few methods have been established to control the size and size distribution effectively,

(5) (a) Penn, R. L.; Banfield, J. F. *Geochim. Cosmochim. Acta* **1999**, *63*, 1549–1557. (b) Banfield, J. F.; Welch, S. A.; Zhang, H. Z.; Ebert, T. T.; Penn, R. L. *Science* **2000**, *289*, 751–754.
(6) Halder, A.; Ravishankar, N. *Adv. Mater.* **2007**, *19*, 1854–1858.
(7) Pacholski, C.; Kornowski, A.; Weller, H. *Angew. Chem., Int. Ed.* **2002**, *41*, 1188–1191.
(8) Yu, J. H.; Joo, J.; Park, H. M.; Baik, S.-I.; Kim, Y. W.; Kim, S. C.; Hyeon, T. *J. Am. Chem. Soc.* **2005**, *127*, 5662–5670.
(9) Cho, K. S.; Talapin, D. V.; Gaschler, W.; Murray, C. B. *J. Am. Chem. Soc.* **2005**, *127*, 7140–7147.
(10) Tang, Z. Y.; Kotov, N. A.; Giersig, M. *Science* **2002**, *297*, 237–240.
(11) Tang, Z. Y.; Zhang, Z. L.; Wang, Y.; Glotzer, S. C.; Kotov, N. A. *Science* **2006**, *314*, 274–278.
(12) Polleux, J.; Pinna, N.; Antonietti, M.; Niederberger, M. *Adv. Mater.* **2004**, *16*, 436–439.
(13) (a) Lisiecki, I.; Pileni, M. P. *J. Am. Chem. Soc.* **1993**, *115*, 3887–3896. (b) Lisiecki, I.; Bjorling, M.; Motte, L.; Ninham, B.; Pileni, M. P. *Langmuir* **1995**, *11*, 2385–2392. (c) Pileni, M. P. *J. Phys. Chem. C* **2007**, *111*, 9019–9038.
(14) Park, B. K.; Jeong, S.; Kim, D.; Moon, J.; Lim, S.; Kim, J. S. *J. Colloid Interface Sci.* **2007**, *311*, 417–424.
(15) (a) Jana, N. R.; Peng, X. G. *J. Am. Chem. Soc.* **2003**, *125*, 14280–14281. (b) Wu, S. H.; Chen, D. H. *J. Colloid Interface Sci.* **2004**, *273*, 165–169.
(16) Han, W. K.; Choi, J. W.; Hwang, G. H.; Hong, S. J.; Lee, J. S.; Kang, S. G. *Appl. Surf. Sci.* **2006**, *252*, 2832–2838.
(17) Mott, D.; Galkowski, J.; Wang, L. Y.; Luo, J.; Zhong, C. J. *Langmuir* **2007**, *23*, 5740–5745.

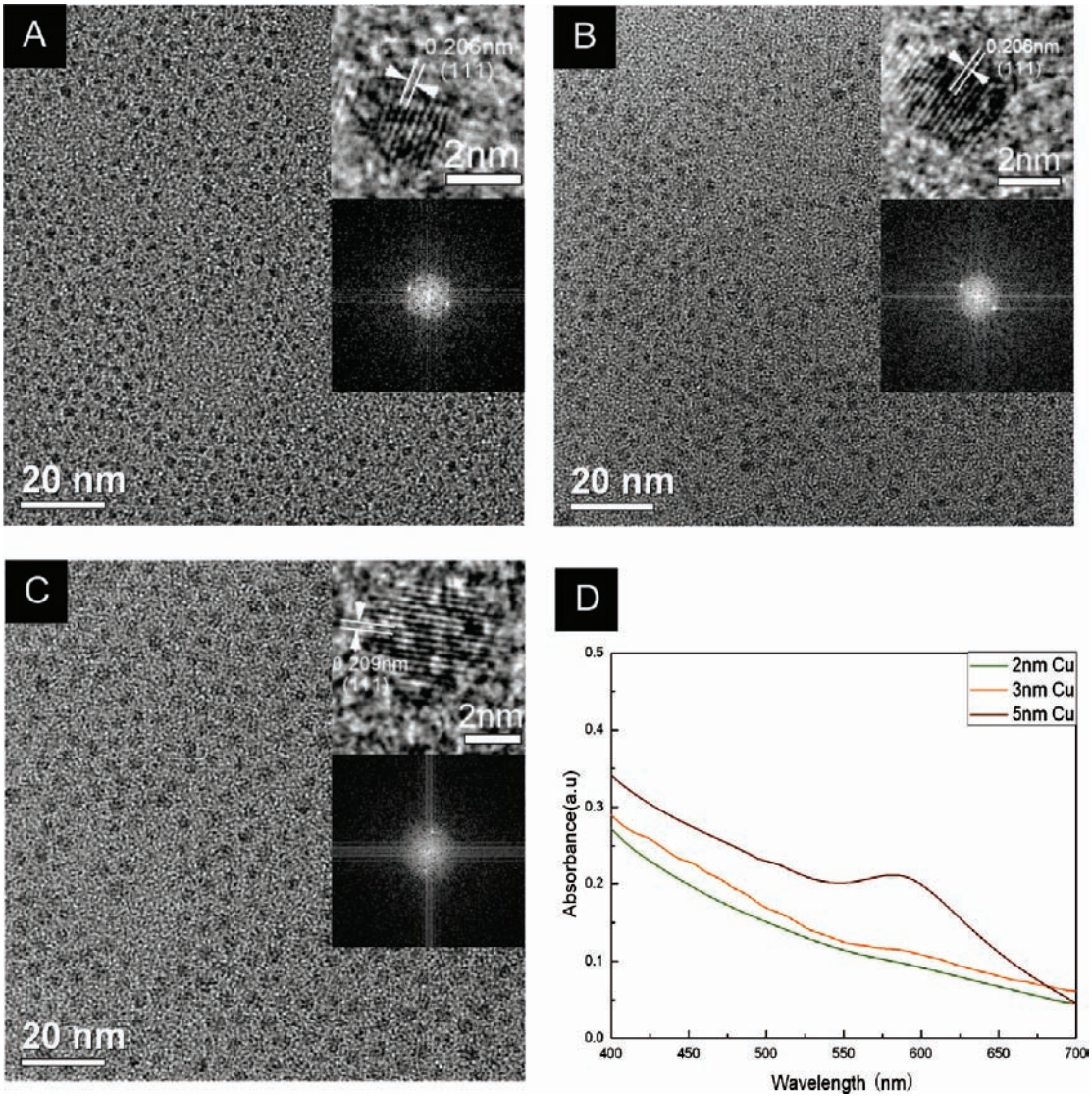


**Figure 1.** TEM images of Cu nanoseeds with different sizes: (a) $2.2 \pm 0.1$ nm, (b) $3.4 \pm 0.1$ nm, and (c) $5.2 \pm 0.2$ nm. The insets are the HRTEM images and the corresponding FFT patterns. (d) Corresponding UV−vis absorption spectra.

because the agglomeration and chaotic growth of Cu particles are often substantial, which leads to the irregular shape and big size. Here, two single-phase approaches were used to precisely control the diameter of Cu nanoseeds. First, the synthesis of 1−4 nm Cu nanoseeds was carried out in a boiling toluene solution containing cationic surfactant (DODA) by using $NaBH_4$ as a reducing reagent. The as-prepared Cu nanocrystals were then coated with DT through ligand exchange. Second, according to a procedure previously developed by Peng and Jana,[15a] Cu nanoseeds about 5 nm in diameter were synthesized in a boiling toluene solution with a fatty acid (OLA) as the surfactant and hydrazine as the reducing reagent. The as-prepared Cu nanocrystals were also coated with DT through ligand exchange.

Figure 1 illustrates the representative TEM images of the obtained Cu nanoseeds. The Cu nanoseeds are all well-dispersed and have a highly uniform size. The lattice spacing in the HRTEM images (inset, Figure 1) of 0.206−0.209 nm calculated by FFT patterns is consistent with the distance of (111) lattice spacing in Cu, revealing the cubic and single-crystalline nature of the nanoseeds. Statistical analysis of the size of the nanoseeds, obtained from counting ~100 nanoseeds from different parts of the grids, indicates that the nanoseeds have an average size of $2.2 \pm 0.1$ nm, $3.4 \pm 0.1$ nm, and $5.2 \pm 0.2$ nm, respectively. Figure 1d shows the UV−visible absorption spectra of the obtained Cu nanoseeds. The surface plasmon peak of small copper nanoseeds (<4 nm) is strongly broadening due to the predominant quantum size effects. When the diameter is larger than 4 nm (5.2 nm), the spectrum exhibits an absorption band at around ~575 nm, which is the typical surface plasmon band of copper nanocrystals.[18]

The size control of Cu nanoseeds was achieved by using DODA or OLA as a capping agent during the formation of the Cu nucleus. The interaction between the outer organic shell and the inner Cu core of Cu-DODA is stronger than that of Cu-OLA, which permits the remaining monomers in the solution to continuously nucleate and, consequently, results in samples full of smaller

(18) Chen, T.Yu .; Chen, S. F.; Sheu, H. S.; Yeh, C. S. *J. Phys. Chem. B* **2002**, *106*, 9717–9722.

**Table 1.** Mode Assignments of DT, OLA, DODA, (Cu-OLA)-DT, and (Cu-DODA)-DT

| peak assignment[a] | DT | OLA | DODA | (Cu-OLA)-DT | (Cu-DODA)-DT |
|---|---|---|---|---|---|
| $\nu_{sym}$(C−H) | 2852 | 2854 | 2849 | 2852 | 2852 |
| $\nu_{asym}$(C−H) | 2922 | 2925 | 2916 | 2932 | 2923 |
| $\delta_s$(C−H) | 1465 | 1465 | 1469 | 1465 | 1465 |
| | 1376 | 1377 | 1374 | 1377 | 1377 |
| $\rho_r(CH_2)n$ | 721 | 723 | 719 | 720 | 721 |
| $\nu$(S−H) | 2570 | | | | |
| $\nu$(C−S) | 654 | | | 652 | 653 |
| $\nu$(C═O) | | 1709 | | | |
| $\nu$(C═C) | | 1412 | | | |
| $\nu$(C−$N^+$) | | | 1079 | | |
| | | | 1055 | | |
| | | | 982 | | |
| | | | 893 | | |
| $\nu(CH_3-N^+)$ | | | 1489 | | |

[a] $\nu$ = stretching, sym = symmetric, asym = antisymmetric, $\delta_s$ = methylene scissoring, $\rho_r$ = rocking.

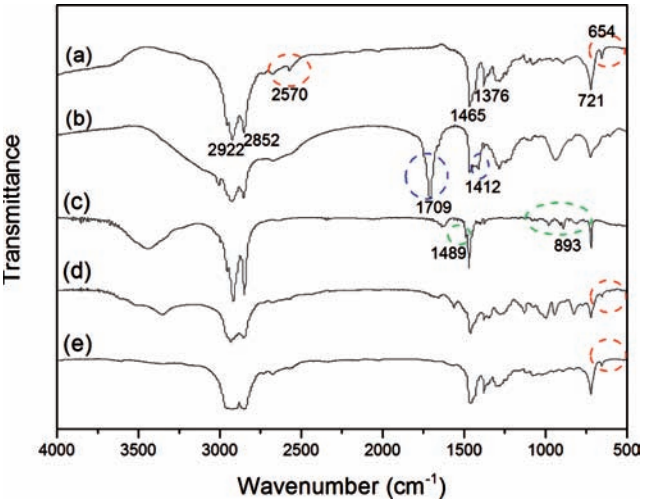


**Figure 2.** FTIR spectra of (a) DT, (b) OLA, (c) DODA, (d) (Cu-OLA)-DT, and (e) (Cu-DODA)-DT.

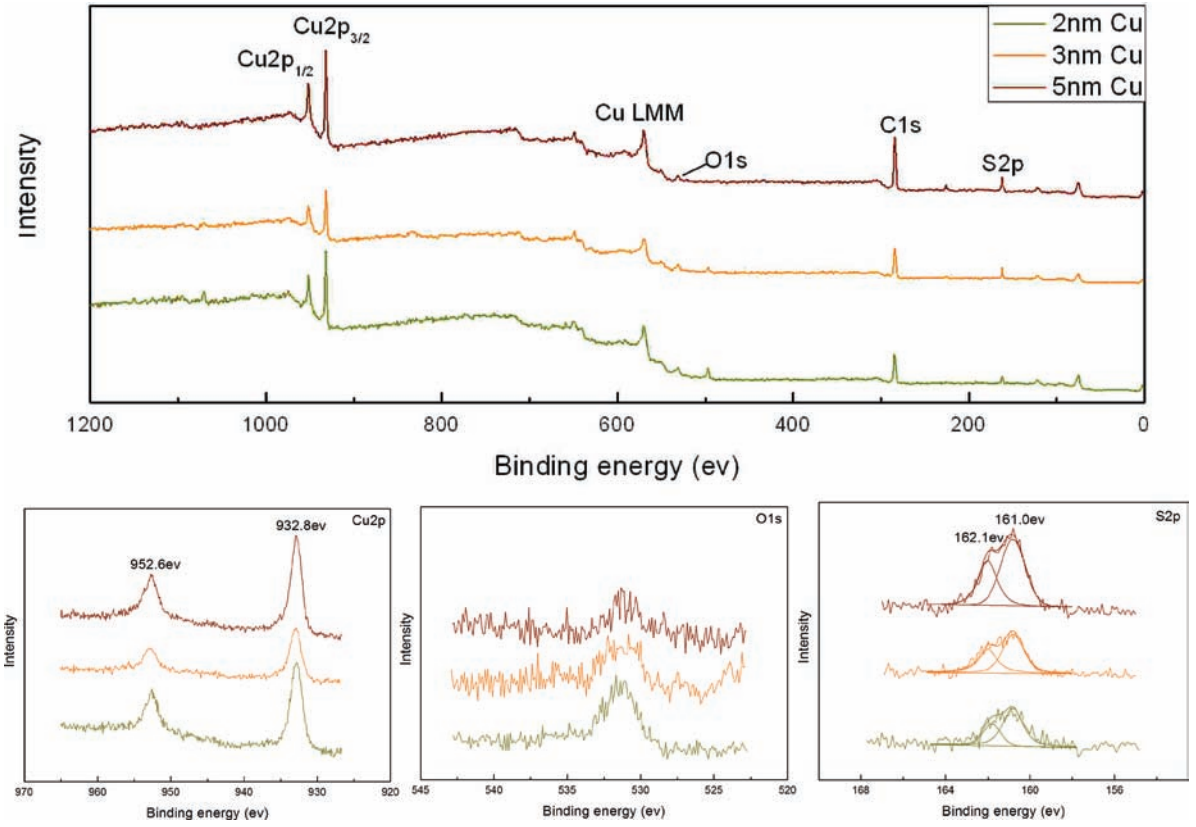


**Figure 3.** XPS spectra of 2, 3, and 5 nm Cu nanoseeds.

particles. The role of DODA and OLA is to control the growth of the Cu nucleus to different extents, and the final stabilizer is DT. DT was chosen as the ultimate stabilizer because it is not only a strong stabilizer capable of preventing the Cu nanoseeds from oxidation and aggregation, but also the sulfur source for the preparation of copper sulfide. DODA and OLA are weaker ligands compared to DT, and the ligand exchange can be achieved straight-away by adding DT into the system containing the as-synthesized Cu nanocrystals coated by DODA or OLA.

More evidence can be obtained from the FTIR spectra of the Cu nanocrystals after ligand exchange by DT, and various peak assignments have been compared in Table 1. (Cu-OLA)-DT and (Cu-DODA)-DT represent Cu nanocrystals synthesized in the presence of OLA and DODA, which are finally exchanged by DT, respectively. Figure 2d indicates that, after ligand exchange, the C═O stretching vibration at 1709 $cm^{-1}$ disappeared. The $CH_3-N^+$ stretching mode at 1489 $cm^{-1}$ and the stretching modes of C−$N^+$ at 1079 $cm^{-1}$, 982 $cm^{-1}$, and 893 $cm^{-1}$ were also absent after ligand

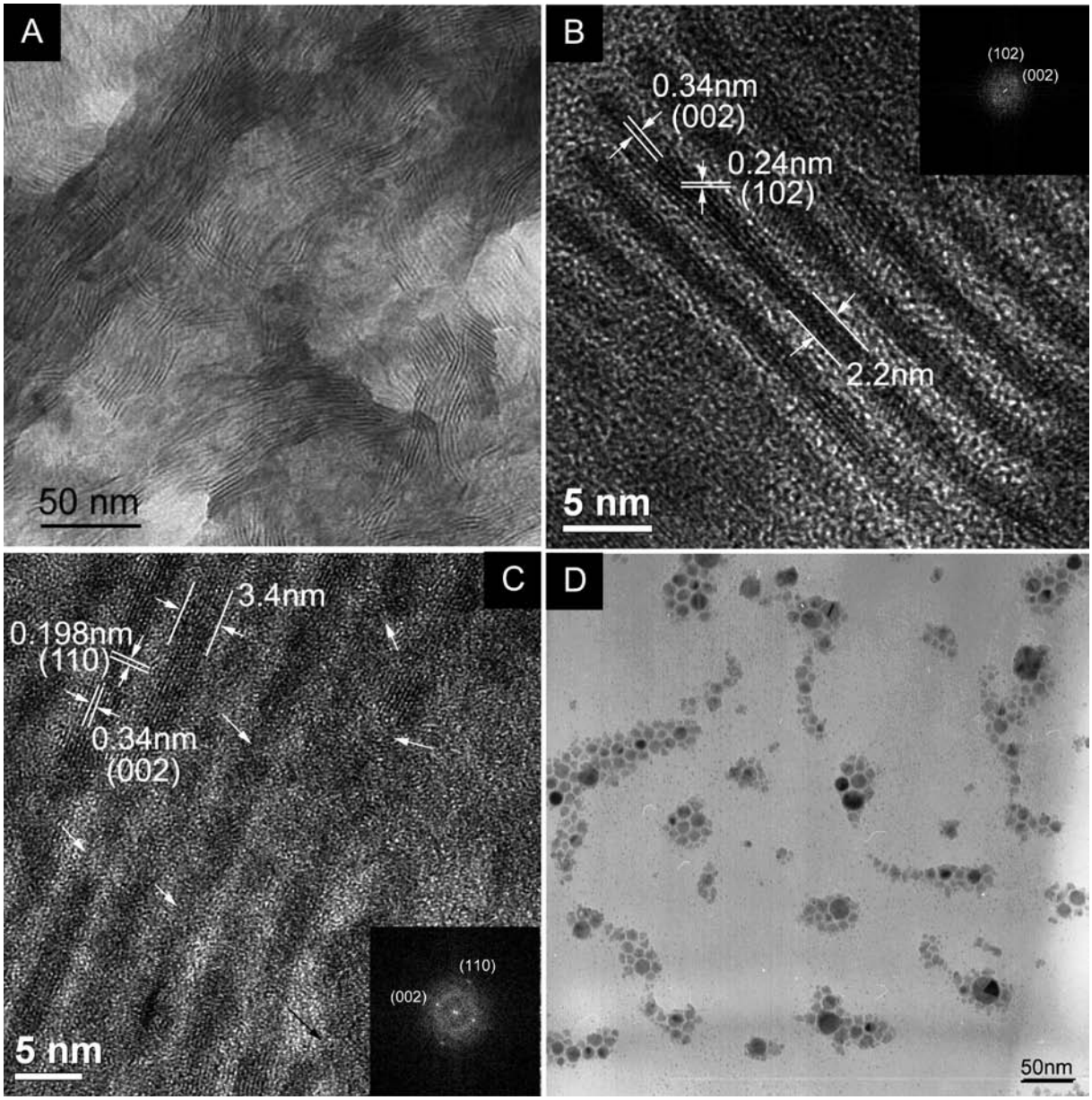


**Figure 4.** (a, b) HRTEM images of $Cu_2S$ nanorods (2.2 nm Cu nanoseeds, 150 °C for 12), (c) HRTEM image of $Cu_2S$ nanorods (3.4 nm Cu nanoseeds, 150 °C for 12), (d) TEM image of $Cu_2S$ particles (5.2 nm Cu nanoseeds, 140 °C for 12 h). Insets are FFT patterns.

exchange (Figure 2e). The stretching vibration of C−S at 600−700 $cm^{-1}$ can be found in Figure 2d and e. This indicates that almost all of the OLA and DODA were exchanged by DT. The absence of S−H stretching vibrations at 2550−2600 $cm^{-1}$ in (Cu-DODA)-DT and (Cu-OLA)-DT implies that S−H is destroyed and S anchors on the surface of Cu nanoseeds with strong interaction.

Detailed information about the surface molecular and electronic structure of the obtained Cu nanoseeds was provided by the XPS analysis. Figure 3 shows the XPS spectra of Cu2p, O1s, C1s, and S2p of the copper surface covered with a monolayer of DT. For all samples, the XPS spectra are similar. The Cu2p3/2 and Cu2p1/2 are detected at 932.8 and 952.6 eV, respectively. The absence of a series of satellite structures of Cu2p3/2 on the high-binding-energy side (934∼943 eV) precludes significant oxidation of the copper nanoseeds in the form of $Cu^{2+}$.[19] The insignificant O1s peaks at ∼531ev indicate that the surface of copper nanoseeds is slightly oxidized in the form of $Cu_2O$. The intensity of O1s increases slightly with the decrease of Cu size due to the dramatic increasing in surface activity. A single S2p doublet at 162.1 eV (S2p3/2) is also observed. The binding energies of these doublets are consistent with thiolate species bonded to the surfaces of metal nanocrystals.[20] These clearly indicate that DT absorbed on the surface of Cu nanoseeds through chemisorption, which prevents the oxidation of the copper surface effectively.

(19) Ghijsen, J.; Tjeng, L. H.; Elp, J. v.; Eskes, H.; Westerink, J.; Sawatzky, G. A. *Phys. Rev. B* **1988**, *38*, 11322–11330.

(20) (a) Castner, D. G.; Hinds, K.; Grainger, D. W. *Langmuir* **1996**, *12*, 5083–5086. (b) Vollmer, S.; Witte, G.; Woll, C. *Langmuir* **2001**, *17*, 7560–7565.

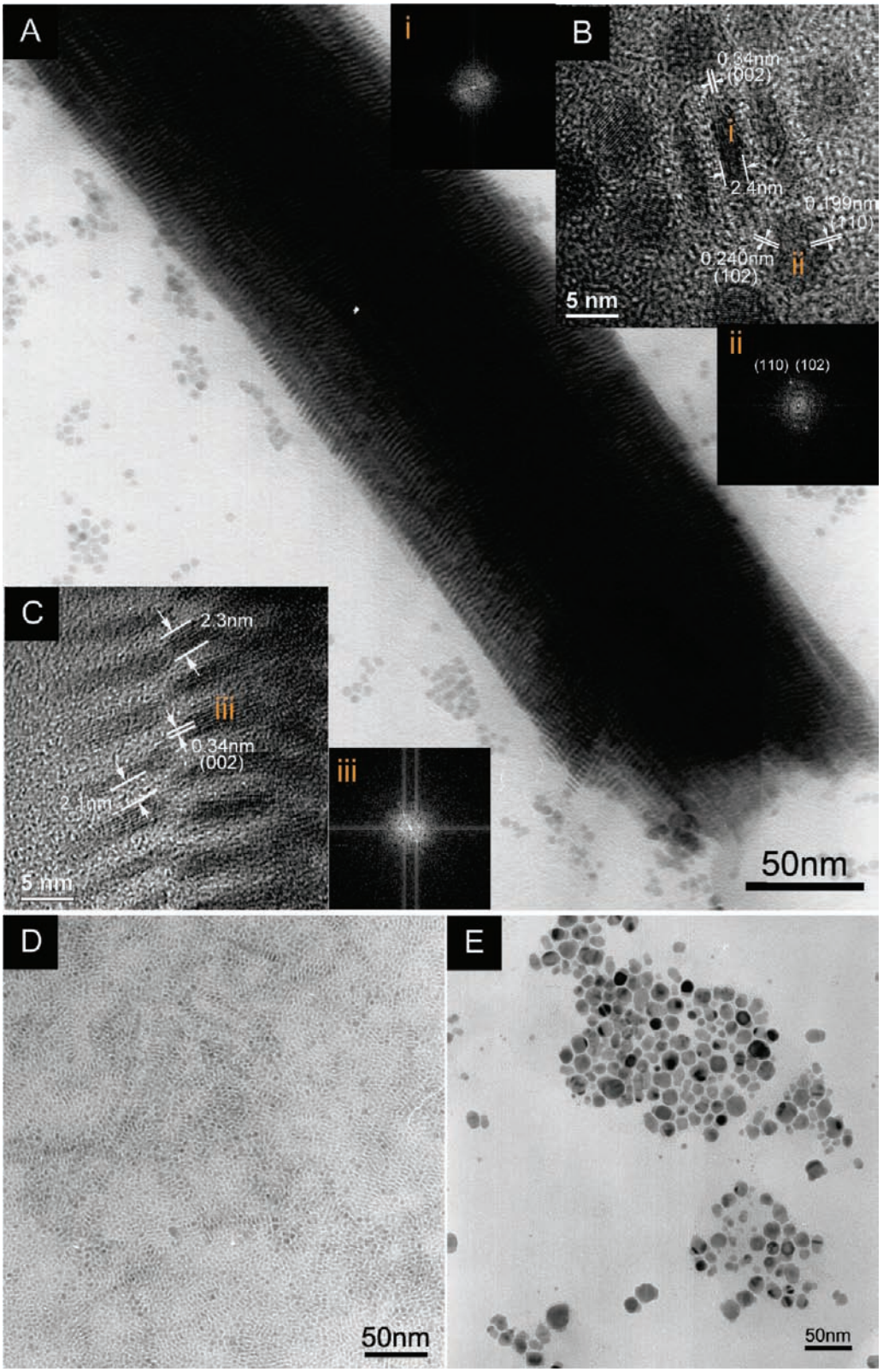


**Figure 5.** (a) TEM image of rodlike $Cu_2S$ superlattice (2.2 nm Cu nanoseeds, 180 °C for 16 h), (b) HRTEM images of unstacked $Cu_2S$ nanodisks, and (c) the edge of rodlike $Cu_2S$ superlattice. (d) $Cu_2S$ nanodisks (3.4 nm Cu nanoseeds, 180 °C for 16 h). (e) $Cu_2S$ particles (5.2 nm Cu nanoseeds, 180 °C for 16 h). i−iii are the FFT patterns of corresponding regions.

**Size Effects in OA Growth Process of Cu Nanoseeds.** TEM investigations were performed to monitor the structural development of Cu nanoseeds. As shown in Figure 4a, the products synthesized from 2.2 nm Cu nanoseeds at 150 °C are composed of many local ordered serpentine nanorods. The HRTEM images (Figure 4b and Figure SI-1a,b in the Supporting Information) show that the nanorods preferentially align with their long axes parallel to each other into separate close-packed "stacks", which is similar to the nematic phase observed

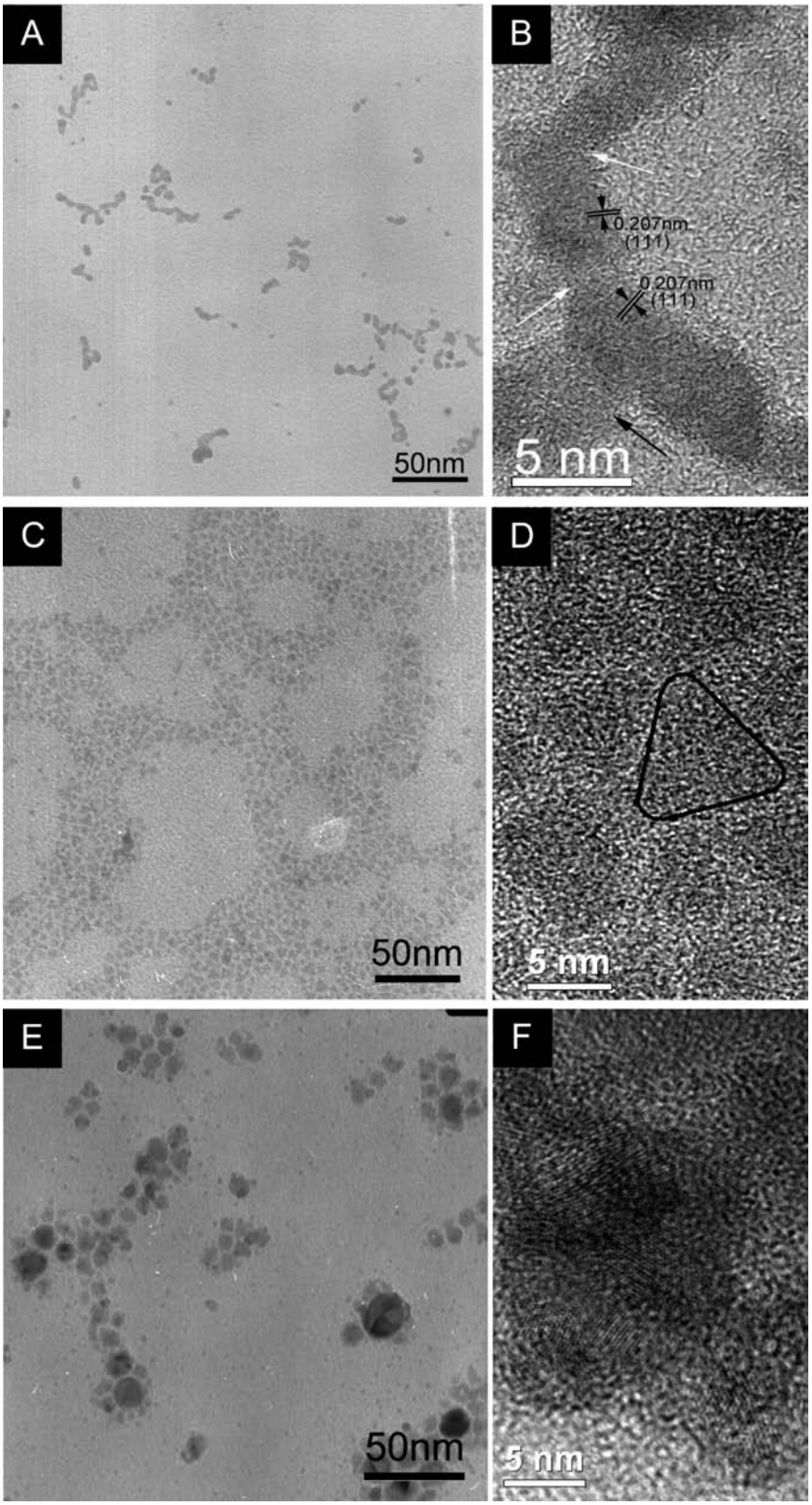


**Figure 6.** TEM and HRTEM images of (a, b) nanocrystal chains (3.4 nm Cu nanoseeds, 140 °C for 8 h), (c, d) disks (3.4 nm Cu nanoseeds, 180 °C for 8 h), and (e, f) particles (5.2 nm Cu nanoseeds, 140 °C for 12 h).

for rodlike colloids in high-volume fractions.[21] The nanorods are single-crystalline $Cu_2S$ in nature, about ~30−100 nm in longitudinal size and 2.2 nm in lateral size. The latter is very close to the diameter of Cu nanoseeds. A similar result has been observed by Tang and co-workers.[10] They reported the self-organization of single CdTe nanoparticles into nanowires controlled

(21) Gelbart, W. M.; Ben-Shaul, A. *J. Phys. Chem.* **1996**, *100*, 13169–13189.

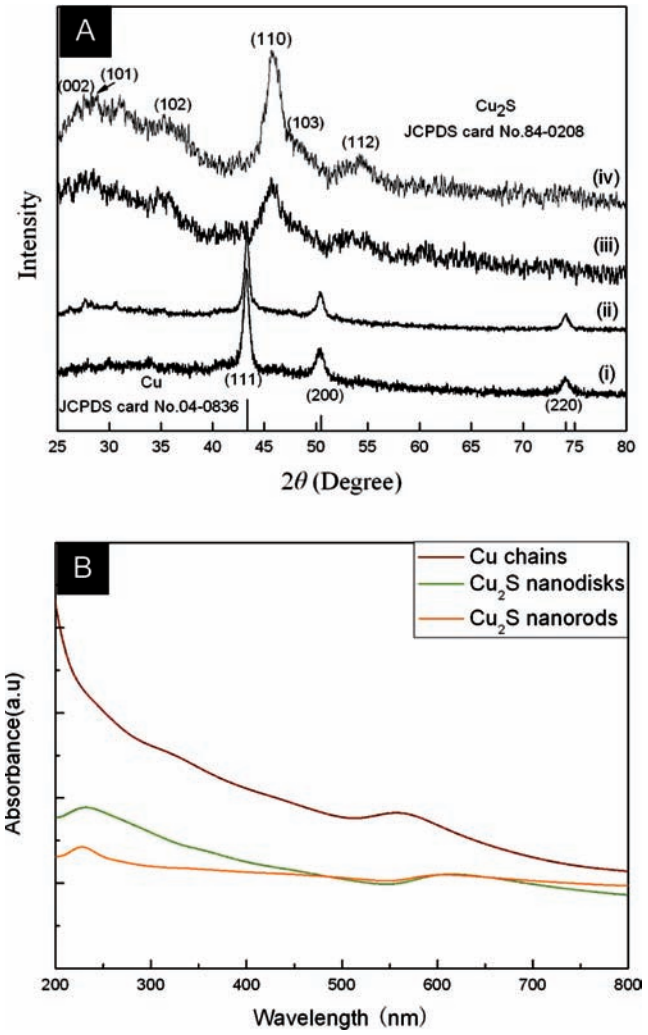


**Figure 7.** (a) XRD patterns of (i) 3.4 nm Cu nanoseeds, (ii) Cu nanocrystal chains (140 °C), (iii) $Cu_2S$ nanorods (150 °C), and (iv) $Cu_2S$ nanodisks (180 °C). The chains, nanorods, and nanodisks are all prepared by using the 3.4 nm Cu nanoseeds. (b) UV−vis absorption spectra of Cu chains, $Cu_2S$ nanorods, and $Cu_2S$ nanodisks.

by strong dipole−dipole interactions and demonstrated that the diameters of the nanowires are virtually identical to the diameters of precursor nanoparticles. As expected, nanorods of about 3.4 nm in width were obtained for 3.4 nm Cu nanoseeds grown under the same conditions. However, more defects (white arrows) and branches (black arrows) can be observed obviously in the nanorods, which makes the rods look intermittent (Figure 4c and Figure SI-1c in the Supporting Information). When the size of the Cu nanoseeds increases up to 5.2 nm, the nanorod is never so much as observed, and only irregular particles with a diameter of 10−20 nm can be obtained (Figure 4d). There are still many small nanoparticles distributed around the bigger particles. This suggests that aggregates of smaller Cu nanoseeds are more ordered and have fewer defects than bigger ones. An important conclusion can be made on the basis of the above results that the morphology of the final $Cu_2S$ nanocrystals was determined by the size of the initial Cu nanoseeds.

When the growth temperature was elevated (180−200 °C), rodlike superlattices with a length of 2−4 $\mu$m and a diameter of 400 nm were obtained from 2.2 nm Cu nanoseeds (Figure SI-2a in the Supporting Information). The TEM and HRTEM images reveal that the as-obtained three-dimensional superlattices are composed of uniform nanodisks with a diameter of 6.5 nm and a thickness of 2.3 nm (Figure 5b), which stack face-to-face perpendicular to the substrate, and the distance between two adjacent nanodisks is about 2.1 nm (Figure 5c). The distance of 2.1 nm, which is shorter than twice the length of the alkyl chains of DT (1.77 nm),[22] suggests that the DT chains are interdigitated during the superlattice formation. In addition to the rodlike superstructures, a few unassembled nanodisks remain to be isolated. Furthermore, the edgewise nanodisks are almost never observed isolated but are usually stacked in lines and made up of a few lying nanodisks sharing their *c* axis (Figure 5b). The plane distances of edgewise nanodisks and lying nanodisks were estimated to be 0.34, 0.24, and 0.199 nm, respectively, which correspond to the (002), (102), and (110) planes of hexagonal $Cu_2S$ nanocrystals. The EDS spectrum (Figure SI-2b in the Supporting Information) confirms that the nanodisks consist of sulfur and copper. Surprisingly, no rodlike superlattices formed, and only unstacked nanodisks (Figure 5d) and irregular particles (Figure 5e) can be obtained by using 3.4 and 5.2 nm Cu nanoseeds, respectively. The above results further confirm the size effects in the growth of Cu nanoseeds.

In fact, the presence of defects in the nanorods and the identical diameter of the nanorods and nanoseeds are characteristic of the OA process. In order to further clarify the formation mechanism of nanorods, nanodisks, and particles, detailed morphological and structural analyses for the early stage of nanorod, nanodisk, and particle formation with different sizes of Cu nanoseeds are shown in Figure 6. As can be seen from Figure 6a, most nanoseeds are self-organized into necklace chains at 140 °C after 8 h from 3.4 nm Cu nanoseeds. The HRTEM image shows that the multimer chain was formed by the alignment of 3.4 nm Cu nanoseeds along the (111) direction. This indication confirms that growth occurred not by monomer deposition but by a coalescence mechanism. It is also worth noting that the multimer chain displays some dislocations (white arrows) and branches (black arrows) in the regions where coalescence occurs. Figure 6c and d show the TEM and HRTEM images of nanodisks at 180 °C for 8 h from 3.4 nm Cu nanoseeds. It can be seen that at this stage the disks are approximately trigonal, suggesting that, in the early stage of reaction, the nanodisks were not grown and crystallized well. Figure 6e and f illustrate the typical morphologies of the agglomerate by the disordered coalescence of 5.2 nm Cu nanoseeds at 140 °C for 12 h, which finally recrystallized into irregular particles (Figure 5e).

XRD measurements (Figure 7a) reveal the occurrence of structural and componential transitions along with the morphology evolution. For the nanoseeds with diameters of 3.4 nm, XRD measurement indicates that they are Cu with a cubic phase, which is very consistent with

(22) Taleb, A.; Petit, C.; Pileni, M. P. *Chem. Mater.* **1997**, *9*, 950–959.

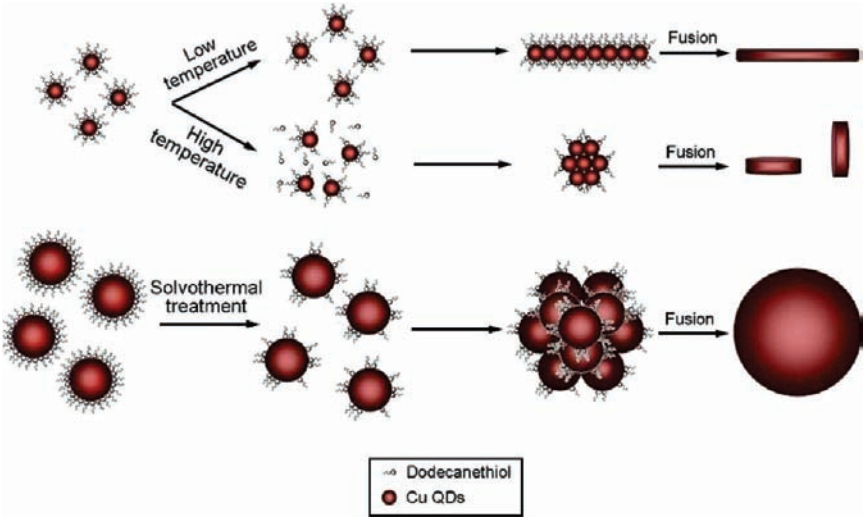


**Figure 8.** Scheme of size effects in the oriented attachment growth process of Cu-DT nanoseeds.

the HRTEM result. Due to the low intensity of O1s (Figure 3), the characteristic peaks of $Cu_2O$ were not detected in XRD measurements. After an OA process at a temperature of 140 °C, necklace structures can be obtained, combining with the HRTEM analysis, which can be indexed to a cubic Cu phase, though the characteristic peaks of $Cu_2S$ emerge in XRD. After treatment at elevated temperatures (150−180 °C), the obtained nanorods or nanodisks can be indexed as hexagonal $Cu_2S$ (JCPDS card No.84−0208), indicating a complete transformation of Cu into $Cu_2S$. For 2.2 and 5.2 nm nanoseeds, similar componential transitions can be observed. The UV−vis adsorption spectra also monitored the optical behavior from Cu-DT to $Cu_2S$ (Figure 7b). The Cu nanochains exhibit the typical adsorption peak of elongated Cu nanocrystals (564 nm).[23] $Cu_2S$ nanorods and nanodisks exhibit significant blue-shift peaks (228 and 231 nm, respectively) in the UV−vis absorption spectrum compared to that of the bulk phase (1022 nm),[24] which shows a quantum size effect. The similar adsorption peaks of $Cu_2S$ nanodisks and nanorods were possibly induced by the identical diameter of nanodisks and nanorods. When the XPS, HRTEM, and XRD results are combined, it can be concluded that DT as the sulfur source of sulfide anchored on the surface of Cu nanoseeds by chemisorption, and then the Cu-DT nanoseeds self-organized into 1D, 2D, or 3D aggregates, which is determined by the size and surface properties of the nanoseeds, and gradually transferred into $Cu_2S$ through controlling solvothermal conditions.

According to the Derjaguin−Landau−Verwey−Overbeek model,[25] the van der Waals interaction ($W_{vdw}$) and ligand steric repulsion ($W_L$), which originated from the steric repulsion of surface-adsorbed DT, are believed to be the dominant forces for the formation of 1D, 2D, and 3D aggregates of Cu-DT nanoseeds. The total interaction potential ($W_T$) is expressed as the sum of $W_L$ and $W_{vdw}$:

$$W_T = W_{vdw} + W_L \quad (1)$$

If the repulsion is weaker than the attraction ($W_T < 0$), nanoseeds aggregate. If the repulsion is stronger than the attraction ($W_T > 0$), nanoseeds disperse.

The energy of the steric repulsion ($W_L$) between two Cu-DT nanoseeds can be expressed by[26]

$$W_L \approx \frac{100R\delta^2}{(C-R)\pi\sigma_{thiol}^3} kT \exp\left(\frac{-\pi(C-R)}{\delta}\right) \quad (2)$$

where $\delta$ is the thickness of the thiol monolayer, $T$ is the temperature, $\sigma_{thiol}$ is the diameter of the area occupied by the thiol on the particle surface, $R$ is the diameter of the nanoseed and $C$ is the distance between the centers of the two nanoseeds. From eq 2, we can see that the higher packing density (i.e., smaller $\sigma_{thiol}$) of DT should correlate with a stronger steric repulsion. On the basis of the above analysis, DT may be dominant and adhere on the (111) facets of Cu nanoseeds. Passivation of the (111) facets lowers the energy of these facets. When the Cu nanoseeds are transferred from the nucleation solution into the solvothermal system, the facets coated with less DT become "defects", which provide the junctures for the attachment of adjacent nanoseeds driven by van der Waals interaction. Generally, surface energy increases dramatically with the decrease of nanoseed diameter due to the obvious increase in the surface-to-volume ratio, which will increase the adsorption of DT on other facets. This is why smaller nanoseeds with less "defects" tend to attach into chain structures. Comparatively, there are many more "defects" distributed on the surface of bigger Cu nanoseeds, and van der Waals forces are known to increase with crystal size, so 2D or 3D structures are easy to obtain. Increasing the solvothermal treatment temperature

(23) Lisiecki, I.; Billoudet, F.; Pileni, M. P. *J. Phys. Chem.* **1996**, *100*, 4160–4166.
(24) Haram, S. K.; Mahadeshwar, A. R.; Dixit, S. G. *J. Phys. Chem.* **1996**, *100*, 5868–5873.
(25) Sinyagin, A. Y.; Belov, A.; Tang, Z. Y.; Kotov, N. A. *J. Phys. Chem. B* **2006**, *110*, 7500–7507.
(26) (a) de Gennes, P. G. *Adv. Colloid Interface Sci.* **1987**, *27*, 189–209. (b) Korgel, B. A.; Fullam, S.; Connolly, S.; Fitzmaurice, D. *J. Phys. Chem. B* **1998**, *102*, 8379–8388. (c) Zhang, S. H.; Leem, G.; Srisombat, L. T.; Lee, R. *J. Am. Chem. Soc.* **2008**, *130*, 113–120.

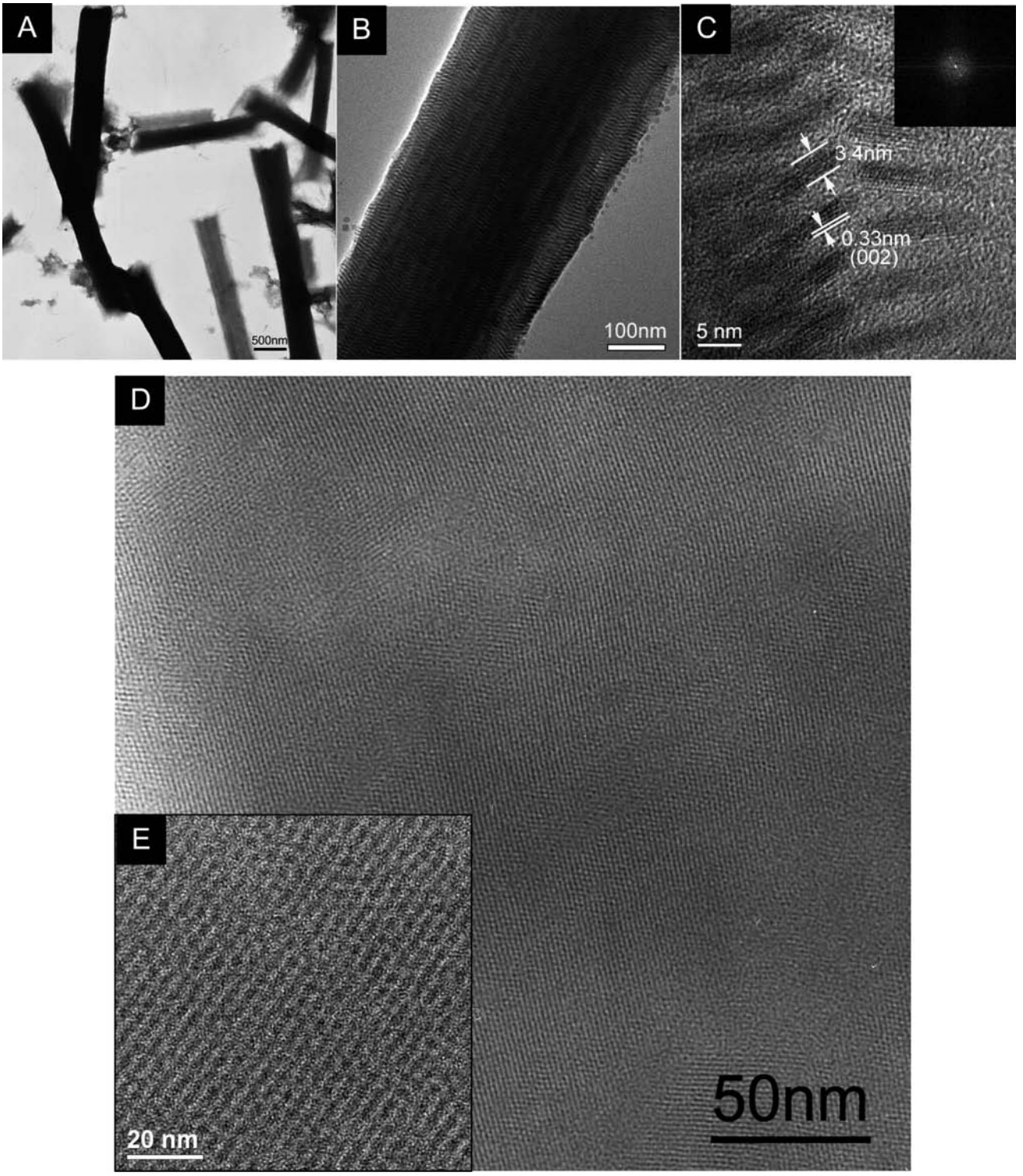


**Figure 9.** TEM and HRTEM images of $Cu_2S$ nanocrystals prepared at different DT concentrations using 3.4 nm Cu nanoseeds at 180 °C. (a−c) 3D rodlike superlattices (0.03% DT). Inset is FFT pattern. (d, e) 2D superlattices (0.12% DT).

quickens the decomposition of copper thiolate; in addition, DT adhered on the (111) facets will be desorbed, which leads to more "defects" appearing. This explains why the smaller nanoseeds can also attach to 2D disks at higher temperatures (Figure 8). Furthermore, for the same size Cu nanoseeds, more "defects" on the surface will result in nonuniform nanocrysals, which can be attested to by the following self-assembly behaviors of $Cu_2S$ nanodisks.

**Surface-Determined OA Process of Cu Nanoseeds.** The formation of $Cu_2S$ nanodisks considerably enhances the long-range dipolar forces compared with isolated Cu nanocrystals, leading to an anisotropic organization. However, the self-assembly of nanocrystals depends to a great extent on homogenization of the building blocks. The uniformity of the unstacked nanodisks (Figure 5d) can be ameliorated by introducing a correct

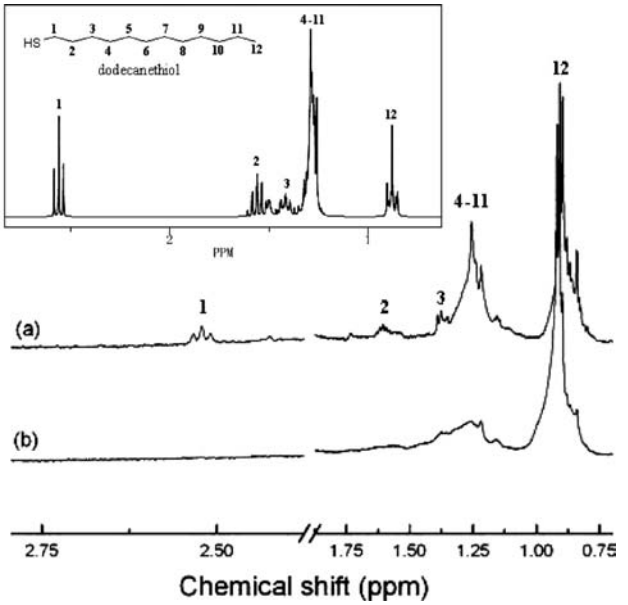


**Figure 10.** $^1$H NMR spectra of $Cu_2S$ nanocrystals in (a) 3D rodlike superlattices and (b) 2D superlattices. Inset: $^1$H NMR spectrum of free dodecanethiol in toluene-$d_8$. The hydrogen numbering is depicted in the upper-left corner.

amount of DT to reduce the "defects" (decrease of $\sigma_{thiol}$) during the solvothermal treatment of 3.4 nm Cu nanoseeds. Figure 9 displays the TEM photographs of the $Cu_2S$ nanocrystals from 3.4 nm Cu nanoseeds at different DT concentrations. When the concentration of DT is 0.03%, three-dimensional rodlike superlattices with a length of 2−4 $\mu$m and a diameter of 400−500 nm can be obtained as shown in Figure 9a−c. The obtained 3D superlattices are composed of face-to-face stacked nanodisks with a diameter of 13 nm and a thickness of 3.5 nm (Figure 9b, c). The distance between two adjacent nanodisks is also about 2 nm. The similarity in distances shows that the energy balance is basically the same as in the 3D superlattices of nanodisks grown from 2.2 nm Cu nanoseeds. It can be seen that almost all of the nanodisks self-assemble into superlattices.

A different close-packed 2D superstructure (Figure 9d) was obtained in the case of adding 0.12% DT. The building blocks in these superlattices are 3.3 nm nanocrystals (Figure 9e), which are similar in size to the initial nanoseeds (3.4 nm). This result indicates that, once there was excess DT in the solution, Cu nanoseeds did not orient into nanorods or nanodisks but experienced a

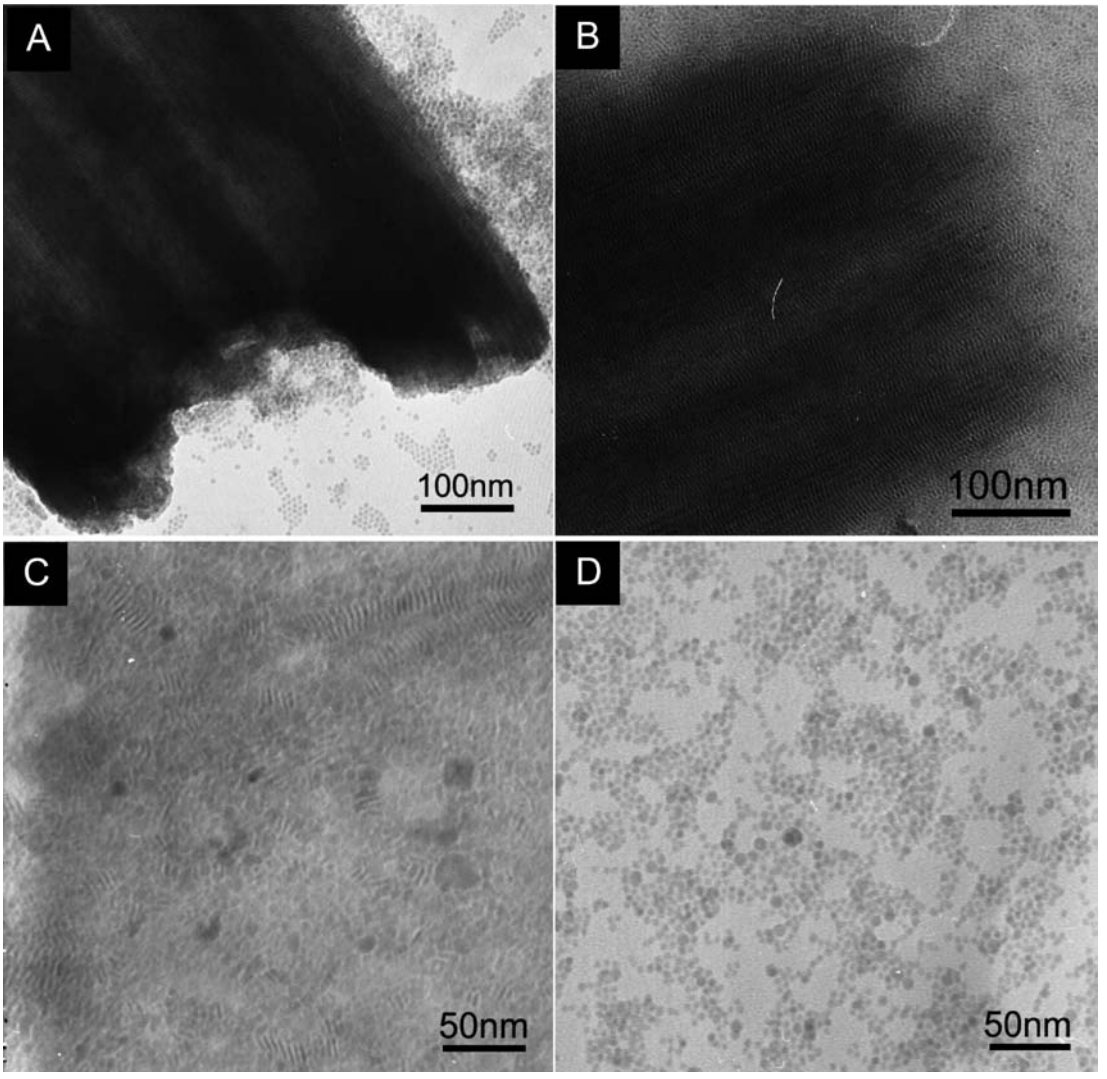


**Figure 11.** TEM images of $Cu_2S$ nanodisks prepared in different solvents using 2.2 nm Cu nanoseeds at 180 °C: (a) toluene, (b) *n*-octane, (c) cyclohexane, and (d) hexane.

digestive ripening procedure,[27] during which the growth was inhibited and narrow size distribution, allowing the nanocrystals to order into a 2D or 3D close-packed array, was achieved.

A comparison of the $^1$H NMR spectra of the $Cu_2S$ nanocrystals in 3D rodlike superlattices and 2D planar superlattices reveals the different capping degrees of DT. The $^1$H NMR spectrum of the nanocrystals in 3D rodlike superlattices shows some broadened peaks and changes in chemical shifts compared to the free dodecanethiol molecules (inset of Figure 10). In fact, resonances of $H_1-H_3$ methylene groups do not appear in the spectrum of nanocrystals in 2D planar superlattices, whereas the resonances assigned to the $H_{12}$ methylene protons remain largely unchanged. This is representative for chemisorbed functional groups on nanocrystal surfaces.[28] Because the $H_1$ atom is closest to the nanocrystal/sulfur interface, it is thus expected to give the broadest peak. Comparatively, the terminal methyl hydrogen (e.g., $H_{12}$ in Cu-DT) experiencing the slowest spin relaxation will have the highest orientation degree of freedom. Thus, the bound dodecanethiol extends into the solvent with a relatively high degree of mobility, which provides the steric stabilization necessary to construct different superstructures. The increase in peak width from curve a to curve b in Figure 10 suggests stronger dipolar interactions and thus a more ordered chain arrangement in the latter.

Similarly, for the smaller Cu nanoseeds (2.2 nm), which can be used to prepare rodlike superlattices, when the other reaction parameters are kept unchanged (180 °C, 16 h), decreasing the density of DT (increase of $\sigma_{thiol}$) will result in the assembled superlattices becoming unstacked nanodisks. Figure 11 illustrates the TEM images of $Cu_2S$ nanodisks synthesized in different solvents by using 2.2 nm Cu nanoseeds. It can be seen that, when toluene is used as a solvent, the rodlike superlattice is very thick with a uniform diameter and the nanodisks are close-packed. When *n*-octane was used to replace toluene as the solvent, rodlike superlattices could also be obtained, but the assembly of nanodisks was loose and there were many more unstacked nanodisks depositing on the substrate. When cyclohexane and hexane were used, nanodisks were almost unstacked and the size distributions of the disks were wide. The solubility of DT in the solvents increases with the decrease of solvents' polarity (toluene > *n*-octane > cyclohexane > hexane). More surface "defects" lead to the formation of irregular disks and decrease the assembly rate. However, there is actually still no model which could quantitatively evaluate this effect.

(27) (a) Prasad, B. L. V.; Stoeva, S. I.; Sorensen, C. M.; Klabunde, K. J. *Chem. Mater.* **2003**, *15*, 935–942. (b) Stoeva, S.; Klabunde, K. J.; Sorensen, C. M.; Dragieva, I. *J. Am. Chem. Soc.* **2002**, *124*, 2305–2311. (c) Smetana, A. B.; Klabunde, K. J.; Sorensen, C. M. *J. Colloid Interface Sci.* **2005**, *284*, 521–526. (d) Hines, M. A.; Scholes, G. D. *Adv. Mater.* **2003**, *15*, 1844–1849.

(28) (a) Chaki, N. K.; Vijayamohanan, K. P. *J. Phys. Chem. B* **2005**, *109*, 2552–2558. (b) Templeton, A. C.; Cliffel, D. E.; Murray, R. W. *J. Am. Chem. Soc.* **1999**, *121*, 7081–7089. (c) Guo, R.; Song, Y.; Wang, G.; Murray, R. W. *J. Am. Chem. Soc.* **2005**, *127*, 2752–2757. (d) Wang, W.; Murray, R. W. *Langmuir* **2005**, *21*, 7015–7022.

## Conclusion

In summary, Cu nanoseeds with narrow size distributions have been synthesized by single-phase approaches. $Cu_2S$ nanorods and nanodisks, as well as their assemblies and particles, have been synthesized by using the obtained Cu nanoseeds under solvothermal conditions. Size effects have been found in the OA growth process of Cu nanoseeds with different sizes, which induced versatile morphologies of final nanocrystals. The surface density of DT also plays an important role in determining the shape and the assembly of final nanocrystals. The present work provides a controllable way to synthesize complex two- and three-dimensional nanodevices, which will have potential applications in electronics, biotechnology, and energy.

**Acknowledgment.** The authors thank Prof. Yadong Li for his help. This work was supported by NSFC (20725102), the Foundation for the Author of National Excellent Doctoral Dissertation of P. R. China, the Program for New Century Excellent Talents of the Chinese Ministry of Education, the Fok Ying Tung Education Foundation (111012), and the State Key Project of Fundamental Research for Nanoscience and Nanotechnology (2006CB932301).

**Supporting Information Available:** HRTEM images of $Cu_2S$ nanorods, SEM image of rodlike superlattice on silicon-wafer surface, and EDS spectrum obtained during SEM operation. This material is available free of charge via the Internet at http://pubs.acs.org.